Mitigation of the seismic response of multi-span bridges using MR dampers: Experimental study of a new SMC-based controller

Omar El-Khoury[1], Chung Kim[2], Abdollah Shafieezadeh[1], Jee Eun Hur[1] and Gwang Hee Heo[3]

Abstract
Pounding between adjacent structures has been a concern in multi-span bridges in recent earthquakes. In this paper, a pounding mitigation strategy using magnetorheological dampers is proposed, and its performance is tested for a three-span bridge using a series of shake-table experiments. A new semi-active control algorithm called SMC-OPC is developed that is based on a clipped sliding mode control (SMC) with sliding surfaces designed using an optimal polynomial control (OPC) approach. The control design uses a stochastically linearized model of the nonlinear bridge with passive components of the magnetorheological dampers embedded to achieve a more representative system characterization. Optimal weighting matrices for the optimal polynomial control are found through a genetic algorithm. The proposed method along with uncontrolled, passive-off, and passive-on cases are tested on shake-tables for several scaled near-field Kobe ground motion records. Although no pounding is observed in all control cases for small earthquakes, significant pounding occurs in the uncontrolled and passive-off systems under large earthquakes. For these ground motions, the performance of the semi-active controller converges to that of the passive-on case but with noticeably reduced power consumption. The study shows that the use of magnetorheological dampers between adjacent spans is very effective in mitigating critical bridge responses especially under large earthquakes. In addition, the proposed SMC-OPC semi-active control strategy enables achieving balance among multiple performance objectives with significantly reduced power consumption as compared to passive-on case.

1. Introduction

The complex behavior of bridges during seismic events and the vulnerabilities of these assets have been extensively studied with the purpose of improving the design and providing cost-effective mitigation options to reduce the potential of various types of damage and catastrophic failures. Primary types of damage that have been studied are shear and flexural failure of columns (Han et al., 2009; Kim et al., 2010), expansion joint failure (Zhang et al., 2008; Raheem, 2009), local failure of hinge bearings (Song and Kim, 2007; Johnson et al., 2008; Saiidi et al., 2012), and deck collapse (Pamuk et al., 2005; Han et al., 2009). To enhance the seismic performance of bridges, various retrofit strategies have been developed such as cable restrainers (DesRoches et al., 2003; Andrawes and DesRoches, 2007; Padgett et al., 2010), column steel jackets (Kim and Shinozuka, 2004), friction pendulum bearings (Dicleli and Mansour, 2003), and carbon fiber

[1]Department of Civil, Environmental, and Geodetic Engineering, Ohio State University, USA
[2]Department of Civil Engineering, Chungnam National University, Korea
[3]Department of Civil Engineering, Konyang University, Korea

Corresponding author:
Gwang Hee Heo, Konyang University, Naedong 26, Nonsan, Chungnam 320-711, Korea.
Email: shafieezadeh.1@osu.edu

reinforced polymers (Yeh and Mo, 2005; Zaghi et al., 2012; Moustafa and Mousalam, 2015). Structural control provides an alternative solution to enhance the safety and serviceability of bridges against moderate to large earthquakes such that these systems can remain operational following earthquakes (Park et al., 2005; Agrawal et al., 2009; Maddaloni et al., 2011; El-Khoury et al., 2015).

Pounding between adjacent decks in multi-span bridges is a type of damage that can impact the functionality of bridges following earthquakes and, therefore, has to be considered in the design of new or retrofit of existing bridges. Moreover, pounding is a complex phenomenon that induces plastic deformation, local cracking, and fracturing (DesRoches et al., 2011; Naserkhaki et al., 2012; Efraimiadou et al., 2013). In multi-span highway bridges, pounding during seismic events may induce minor (concrete crushing) to major (span unseating) damage (Kawashima et al., 2009; Huo and Zhang, 2012; Won et al., 2015). Structural control is a possible solution to the problem of pounding of adjacent structures (Zou et al., 2012). In addition to its ability to mitigate pounding, it can minimize other key responses of interest such as column displacement and deck acceleration (Abdel-Rohman and John., 2006; Guo et al., 2009; Huo et al., 2012; Basili et al., 2013; Saaed et al., 2015). In that respect, magnetorheological (MR) dampers are employed that exhibit desirable features such as robustness, stability, adaptability, and low power requirements as compared to active and passive-on (input current set at maximum value) systems (Agrawal et al., 2003; Leavitt et al., 2006; Yang and Cai, 2015). However, a primary challenge in designing control algorithms for this type of semi-active dampers arises from the nonlinear behavior of the device and the constraints on achievable control forces. An approach to overcome this complexity is to use clipped optimal control designs based on sliding mode control (SMC) method.

The SMC algorithm is not based on a minimization procedure such as those in conventional optimal feedback control methods, and the design of the sliding surface is a subjective procedure that relies heavily on the experience of the designer. For instance, Yang et al. (1994) introduced linear sliding surfaces based on a regular form transformation and a linear quadratic regulator (LQR) methodology. The surface designs were analyzed on linear elastic systems (Yang et al., 1995a) and hysteretic systems (Yang et al., 1995b). The control design showed noticeable improvements, and robustness was examined and verified by varying the structural stiffness within 10%. Yang et al. (1996) tested the sliding surface design for a seismically excited building and showed that the SMC design provides better peak response

reduction as compared to traditional feedback LQR control algorithms.

However, the control law presented by Yang et al. (1994) cannot be achieved unless the external excitation is known in advance. To address this issue, Adhikari and Yamaguchi (1997) replaced the excitation dependent feedforward component by a Heaviside function that compensates for effects of stochastic disturbances and enhances the stability of the system. The Heaviside component is a source of chattering which causes damage to mechanical components. As a result, this discontinuous component was replaced by a smooth tangent-hyperbolic function. These design strategies were shown to performance well in terms of reducing peak responses in actively and semi-actively controlled multistory buildings (Guclu, 2006; Wang and Lin, 2007; Fan et al., 2009) and bridges (Lee and Chen, 2011a, 2011b). However, implemented linear sliding surfaces restrict the control performance in terms of response reduction and control force minimization for nonlinear systems. In this paper, a new approach is developed to design SMC controllers based on a nonlinear feedback optimal polynomial control (OPC) that generalizes LQRs to include higher order terms. The control algorithm, called sliding mode control based on OPC (SMC-OPC), is expected to yield better peak response reduction compared to linear SMC surface design at no additional cost. In general, the proposed semi-active control design is intended to provide a balance between the performance of the controlled system and the power consumption of the controller. The former objective relates to the serviceability and reliability of the structural systems, whereas the latter one corresponds to the performance of the control device (Bajaj et al., 2014). In this respect, during large seismic events where safety and reliability of the bridge is the major concern, the performance of the semi-active controller converges to that of the passive-on controller but with considerably reduced power consumption.

The proposed semi-active control algorithm is analyzed and tested using shake-table tests on a three-span bridge with a total length of 12.0 m equipped with two MR dampers attached between adjacent spans. A comprehensive step-by-step procedure is presented for the control design. This is followed by modeling nonlinear bridge components to capture hysteretic responses and pounding. Then, a statistical linearization approach is implemented to provide an equivalent linear model, while accounting for the uncertainty in the system response owing to seismic disturbances. Next, clipped-optimal SMC is designed according to a second-level optimization that determines the optimal semi-positive definite weighting matrices. The design is tested using

shake-table tests of a three-span bridge subjected to a scaled Kobe ground motion (denoted by KB). In the testing procedure, the MR dampers are set to minimum and maximum current values, as well as the optimal current determined from semi-active control strategy. The results are elaborated for small- and large-scaled Kobe earthquake ground motions at different controlled states: uncontrolled structure (the bridge without MR dampers), passive-off (where the input current is set to zero at all times during earthquakes), passive-on (where the input current is set to maximum value at all times during earthquakes), and semi-active case (in which the input current ranges between minimum and maximum values according to the proposed clipped SMC-OPC algorithm).The performance of these control cases is compared based on maximum absolute displacements of the decks, maximum relative displacements between adjacent deck segments and between deck segments and abutments, and finally the maximum absolute acceleration of deck segments. A primary control objective is to reduce maximum relative displacements that control the likelihood of damage owing to pounding. Another goal of the control system is to reduce the maximum absolute displacements and the peak accelerations in order to mitigate damage to supports (Johnson et al., 2008; Saiidi et al., 2012) and enhance riding comfort (Kwon et al., 1998; Ni et al., 2001; Yau, 2009). The different control cases of the MR dampers considered in this study exhibit various attributes such as the adaptability to earthquake characteristics and the reduced power consumption in semi-active state, the suboptimal response reduction in passive-on state, and the functionality of the MR dampers when no power is available in the passive-off state.

The rest of this paper is organized as follows. Section 2 presents a detailed derivation of the novel control algorithm called SMC-OPC for the semi-active control of the system. Next, characteristics of the case study bridge along with modeling techniques for the rubber bearings, MR dampers, and pounding behavior and their validation with experimental results are explained in Section 3. Section 4 describes the procedure for stochastic linearization of the system and optimization of the clipped semi-active control design. Shake table experiment results for the proposed SMC-OPC method along with uncontrolled, passive-on, and passive-off cases are presented in Section 5. Conclusions of the research are summarized in Section 6.

2. Nonlinear sliding mode control

In this section, a state-space based nonlinear SMC-OPC is initially derived for the active control of a fully observable system. Then, the considerations of semi-active control and partial observability are accounted in the design implementation for the particular system in Section 4. In that respect, a general linearized system subjected to stochastic disturbance is assumed and represented in state-space model as

$$\dot{\mathbf{X}} = G(\mathbf{X}, \mathbf{u}, t) = \mathbf{A_{state}}\mathbf{X} + \mathbf{B}\mathbf{u} + \mathbf{F_e} \qquad (1)$$

where $\mathbf{X}$ is the response vector and $\mathbf{A_{state}}$ is the system matrix which is derived using mass, damping, and stiffness components of the dynamic system. In addition, the system matrix can include models for the dynamics of the passive-off component of the control device and stochastically linearized models for the nonlinear behavior of the system. In equation (1), $\mathbf{F_e}$ and $\mathbf{B}$ represent the excitation vector and the location matrix of controllers. The control component, $\mathbf{u}$, denotes the force vector applied by active or semi-active controller. Unlike the case in conventional LQR and Linear Quadratic Gaussian (LQG) methods, the design of SMC is not based on a minimization procedure. Instead, the SMC design is known to be a two-step procedure. The first step involves the design of the sliding surface. Then, a control law is selected to drive the response variables to the defined sliding surface. In order to design linear SMC forces, an optimal sliding surface can be obtained based on minimizing a LQR performance index, L_{LQR}, with semi-positive weighting matrix, $\mathbf{Q}_1$

$$L_{\mathrm{LQR}} = \int_0^\infty \mathbf{X^T}\mathbf{Q}_1\mathbf{X}\mathrm{d}t \qquad (2)$$

The corresponding linear sliding surface is represented by

$$\mathbf{S} = \mathbf{P}\mathbf{X} \qquad (3)$$

where $\mathbf{P}$ is to be determined according to LQR method in order to force the system state trajectory to move along a stable manifold (Utkin, 1992; Yang et al., 1994; Adhikari and Yamaguchi, 1997). To enhance the transient response, this study proposes extending the sliding surface to include higher order nonlinear terms; this extension is expected to improve vibration mitigation of the system. As a result, the performance index is expanded to include higher order terms (HOT) to

$$L_{\mathrm{OPC}} = \int_0^\infty \big(\mathbf{X^T}\mathbf{Q}_1\mathbf{X} + \mathrm{HOT}\big)\mathrm{d}t \qquad (4)$$

where the terms, $\mathbf{Q}_1$ and HOT are defined later in equation (19). First, to design the sliding surface, the

state-space system in equation (1) is converted into the so-called regular form of transformation (Utkin, 1992). The converted system of the state space vector, $\mathbf{Y}$, is represented by

$$\dot{\mathbf{Y}} = \hat{\mathbf{A}}_{\mathbf{state}}\mathbf{Y} + \hat{\mathbf{B}}\mathbf{u} + \hat{\mathbf{F}}_{\mathbf{e}}, \quad \mathbf{Y} = \mathbf{D}\mathbf{X} \tag{5}$$

where $\mathbf{D}$ is the orthogonal transformation matrix. The system is transformed and represented with new state-space system, defined by $\hat{\mathbf{A}}_{\mathbf{state}}$ $(= \mathbf{D}\mathbf{A}_{\mathbf{state}}\mathbf{D}^{-1})$, $\hat{\mathbf{B}}$ $(= \mathbf{D}\mathbf{B})$, $\hat{\mathbf{F}}_{\mathbf{e}}$ $(= \mathbf{D}\mathbf{F}_{\mathbf{e}})$. The new system matrices can be partitioned as

$$\mathbf{Y} = \left\{ \begin{array}{c} \mathbf{Y}_1 \\ \mathbf{Y}_2 \end{array} \right\}, \quad \hat{\mathbf{A}}_{\mathbf{state}} = \left[\begin{array}{cc} \hat{\mathbf{A}}_{\mathbf{state}_1} & \hat{\mathbf{A}}_{\mathbf{state}_{12}} \\ \hat{\mathbf{A}}_{\mathbf{state}_{21}} & \hat{\mathbf{A}}_{\mathbf{state}_2} \end{array} \right],$$
$$\hat{\mathbf{B}} = \left[\begin{array}{c} 0 \\ \mathbf{B}_{\mathbf{T}} \end{array} \right] \quad \text{and} \quad \hat{\mathbf{F}}_{\mathbf{e}} = \left\{ \begin{array}{c} \hat{\mathbf{F}}_{\mathbf{e}_1} \\ \hat{\mathbf{F}}_{\mathbf{e}_2} \end{array} \right\} \tag{6}$$

where $\mathbf{B}_{\mathbf{T}}$ is the transformed sub-location matrix. Assuming that the vector, Y, is an N-dimensional transformed response vector and u is a P-dimensional control force vector, the vector, $\mathbf{Y}_1$, includes the $(N\text{-}P)$ components that are independent of the control force. The remaining P components of Y form the vector $\mathbf{Y}_2$. This approach enables designing a state space-based surface that is explicitly a function of only $\mathbf{Y}_1$ and $\mathbf{Y}_2$. As a result, the system in equation (5) can be rewritten as

$$\dot{\mathbf{Y}}_1 = \hat{\mathbf{A}}_{\mathbf{state}_1}\mathbf{Y}_1 + \hat{\mathbf{A}}_{\mathbf{state}_{12}}\mathbf{Y}_2 + \hat{\mathbf{F}}_{\mathbf{e}_1} \tag{7a}$$

$$\dot{\mathbf{Y}}_2 = \hat{\mathbf{A}}_{\mathbf{state}_{21}}\mathbf{Y}_1 + \mathbf{B}_{\mathbf{T}}\mathbf{u} + \hat{\mathbf{A}}_{\mathbf{state}_2}\mathbf{Y}_2 + \hat{\mathbf{F}}_{\mathbf{e}_2} \tag{7b}$$

In the design of the sliding surface using OPC, $\mathbf{Y}_1$ and $\mathbf{Y}_2$ play the role of the state vector and the control force of a traditional system, respectively. The term $\hat{\mathbf{A}}_{\mathbf{state}_{12}}\mathbf{Y}_2$ can be considered virtually as a control force and substituted by $\mathbf{B}'\mathbf{u}'$, therefore

$$\dot{\mathbf{Y}}_1 = \hat{\mathbf{A}}_{\mathbf{state}_1}\mathbf{Y}_1 + \mathbf{B}'\mathbf{u}' + \hat{\mathbf{F}}_{\mathbf{e}_1} \tag{7c}$$

where $\mathbf{B}'$ is the location matrix and $\mathbf{u}'(= \mathbf{Y}_2)$ is the virtual control force. Referring to El-Khoury et al. (2015), the performance index of system in equation (7a) is represented by

$$L_{OPC} = \int_0^\infty \left(\mathbf{Y}_1^{\mathbf{T}}\mathbf{Q}_{11}\mathbf{Y}_1 + \mathbf{Y}_2^{\mathbf{T}}\mathbf{Q}_{22}\mathbf{Y}_2 + (\mathbf{Y}_1^{\mathbf{T}}\mathbf{M}\mathbf{Y}_1)(\mathbf{Y}_1^{\mathbf{T}}\mathbf{Q}_{33}\mathbf{Y}_1) \right. $$
$$\left. + \bar{h}(\mathbf{Y}_1) \right)\mathrm{d}t \tag{8}$$

The semi-positive definite matrices, $\mathbf{Q}_{11}$, $\mathbf{Q}_{22}$, and $\mathbf{Q}_{33}$ are gain components. The relationship of these gains

with the matrices in equation (4) is shown later in equations (18) and (19). The term, $\bar{h}(\mathbf{Y}_1)$, is defined as

$$\bar{h}(\mathbf{Y}_1) = (\mathbf{Y}_1^{\mathbf{T}}\mathbf{M}\mathbf{Y}_1)\mathbf{Y}_1^{\mathbf{T}}\mathbf{M}.\hat{\mathbf{A}}_{\mathbf{state}_{12}}^{\mathbf{T}}\mathbf{Q}_{33}^{-1}.(\mathbf{Y}_1^{\mathbf{T}}\mathbf{M}\mathbf{Y}_1)\mathbf{M}\mathbf{Y}_1 \tag{9}$$

The virtual OPC force is derived as

$$\mathbf{u}' = \mathbf{Y}_2 = -\mathbf{Q}_{22}^{-1}\hat{\mathbf{A}}_{\mathbf{state}_{12}}^{\mathbf{T}}\mathbf{P}\mathbf{Y}_1 + \mathbf{Q}_{22}^{-1}\hat{\mathbf{A}}_{\mathbf{state}_{12}}^{\mathbf{T}}(\mathbf{Y}_1^{\mathbf{T}}\mathbf{M}\mathbf{Y}_1)\mathbf{M}\mathbf{Y}_1 \tag{10}$$

in which the Ricatti matrix, $\mathbf{P}$, and $\mathbf{M}$ are determined as

$$\mathbf{P}\hat{\mathbf{A}}_{\mathbf{state}_{11}}^{\mathbf{T}} + \hat{\mathbf{A}}_{\mathbf{state}_{11}}^{\mathbf{T}}\mathbf{P} - \mathbf{P}\hat{\mathbf{A}}_{\mathbf{state}_{12}}^{\mathbf{T}}\mathbf{Q}_2^{-1}\hat{\mathbf{A}}_{\mathbf{state}_{12}}^{\mathbf{T}}\mathbf{P} + \mathbf{Q}_{11} = 0$$
$$0 = \mathbf{M}\left(\hat{\mathbf{A}}_{\mathbf{state}_{11}} - \hat{\mathbf{A}}_{\mathbf{state}_{12}}^{\mathbf{T}}\mathbf{Q}_{22}^{-1}\mathbf{A}_{12}^{\mathbf{T}}\mathbf{P} \right)$$
$$+ \left(\hat{\mathbf{A}}_{\mathbf{state}_{11}} - \hat{\mathbf{A}}_{\mathbf{state}_{12}}^{\mathbf{T}}\mathbf{Q}_{22}^{-1}\mathbf{A}_{12}^{\mathbf{T}}\mathbf{P} \right)^{\mathbf{T}}\mathbf{P} + \mathbf{Q}_{33} \tag{11}$$

The condition in equation (10) can be enforced through a sliding surface, $\mathbf{S}$, that satisfies the stability condition ($\mathbf{S} = 0; \dot{\mathbf{S}} = 0$) according to the Utkin–Drazenovic method (Utkin, 1992). This surface can be defined by

$$\mathbf{S} = \mathbf{Y}_2 + \mathbf{Q}_{22}^{-1}\hat{\mathbf{A}}_{\mathbf{state}_{12}}^{\mathbf{T}}\mathbf{P}\mathbf{Y}_1 + \mathbf{Q}_{22}^{-1}\hat{\mathbf{A}}_{\mathbf{state}_{12}}^{\mathbf{T}}(\mathbf{Y}_1^{\mathbf{T}}\mathbf{M}\mathbf{Y}_1)\mathbf{M}\mathbf{Y}_1 \tag{12}$$

Differentiating the sliding surface in equation (12) with respect to time, $\dot{\mathbf{S}}$ is

$$\dot{\mathbf{S}} = \dot{\mathbf{Y}}_2 + \mathbf{Q}_{22}^{-1}\hat{\mathbf{A}}_{\mathbf{state}_{12}}^{\mathbf{T}}\mathbf{P}\dot{\mathbf{Y}}_1 + \dot{f}(\mathbf{Y}_1) \tag{13}$$

where $f(\mathbf{Y}_1)$ equals $\mathbf{Q}_{22}^{-1}\hat{\mathbf{A}}_{\mathbf{state}_{12}}^{\mathbf{T}}(\mathbf{Y}_1^{\mathbf{T}}\mathbf{M}\mathbf{Y}_1)\mathbf{M}\mathbf{Y}_1$ and $\dot{f}(\mathbf{Y}_1)$ $(d\!f(\mathbf{Y}_1)/dt)$ is the time differential. Substituting equations (7a) and (7b) into equation (13), $\dot{\mathbf{S}}$ can be derived as

$$\dot{\mathbf{S}} = \left(\hat{\mathbf{A}}_{\mathbf{state}_{21}}\mathbf{Y}_1 + \mathbf{B}_{\mathbf{T}}\mathbf{u} + \hat{\mathbf{A}}_{\mathbf{state}_2}\mathbf{Y}_2 + \hat{\mathbf{F}}_{\mathbf{e}}2 \right)$$
$$+ \mathbf{Q}_{22}^{-1}\hat{\mathbf{A}}_{\mathbf{state}_{12}}^{\mathbf{T}}\mathbf{P}\left(\hat{\mathbf{A}}_{\mathbf{state}_1}\mathbf{Y}_1 + \hat{\mathbf{A}}_{\mathbf{state}_{12}}\mathbf{Y}_2 + \hat{\mathbf{F}}_{\mathbf{e}_1} \right) + \dot{f}(\mathbf{Y}_1) \tag{14}$$

This equation can be rearranged as

$$\dot{\mathbf{S}} = \left[\begin{array}{cc} \mathbf{Q}_{22}^{-1}\hat{\mathbf{A}}_{\mathbf{state}_{12}}^{\mathbf{T}}\mathbf{P} & 1 \end{array} \right]\left[\begin{array}{cc} \hat{\mathbf{A}}_{\mathbf{state}_1} & \hat{\mathbf{A}}_{\mathbf{state}_{12}} \\ \hat{\mathbf{A}}_{\mathbf{state}_{21}} & \hat{\mathbf{A}}_{\mathbf{state}_2} \end{array} \right]\left\{ \begin{array}{c} \mathbf{Y}_1 \\ \mathbf{Y}_2 \end{array} \right\}$$
$$+ \mathbf{B}_{\mathbf{T}}\mathbf{u} + \left[\begin{array}{cc} \mathbf{Q}_{22}^{-1}\hat{\mathbf{A}}_{\mathbf{state}_{12}}^{\mathbf{T}}\mathbf{P} & 1 \end{array} \right]\left\{ \begin{array}{c} \hat{\mathbf{F}}_{\mathbf{e}}1 \\ \hat{\mathbf{F}}_{\mathbf{e}}2 \end{array} \right\} + \dot{f}(\mathbf{Y}_1) \tag{15}$$

For the convergence of sliding surface, equation (15) is equated to zero. Next, substituting

$$= \left\{ \begin{matrix} \mathbf{Y}_1 \\ \mathbf{Y}_2 \end{matrix} \right\}, \quad \hat{\mathbf{F}}_e = \left\{ \begin{matrix} \hat{\mathbf{F}}_e 1 \\ \hat{\mathbf{F}}_e 2 \end{matrix} \right\}, \quad \boldsymbol{D}_{00} = \left[\boldsymbol{Q}_{22}^{-1} \hat{\mathbf{A}}_{\mathbf{state}_{12}}^{\mathbf{T}} \mathbf{P} \quad 1 \right],$$

$$\text{and} \quad \hat{\mathbf{A}}_{\mathbf{state}} = \begin{bmatrix} \hat{\mathbf{A}}_{\mathbf{state}_1} & \hat{\mathbf{A}}_{\mathbf{state}_{12}} \\ \hat{\mathbf{A}}_{\mathbf{state}_{21}} & \hat{\mathbf{A}}_{\mathbf{state}_2} \end{bmatrix}$$

the control force, **u**, becomes

$$\mathbf{u} = -\mathbf{B}_{\mathbf{T}}^{-1} \left(\boldsymbol{D}_{00} \hat{\mathbf{A}}_{\mathbf{state}} \mathbf{Y} + \boldsymbol{D}_{00} \hat{\mathbf{F}}_e + \dot{f}(\mathbf{Y}_1) \right) \quad (16)$$

The control force in equation (15) works ideally for an external disturbance, $\hat{\mathbf{F}}_e$, that is known a priori. However, for the case of seismic excitations, $\hat{\mathbf{F}}_e$ is not known prior to the occurrence. Therefore, the term, $\hat{\mathbf{F}}_e$, is dropped and is replaced by a properly selected parameter, μ (≥ 0), so that the reachability of the sliding mode is guaranteed with the condition of $\mathbf{S}\dot{\mathbf{S}} = 0$ (Adhikari and Yamaguchi, 1997). It is common that μ is considered to be a percentage of the inertial force ($\mu = \epsilon m\ddot{x}_g, 0 \leq \epsilon \leq 1$). In this approach, the SMC-OPC control force is adjusted to

$$\mathbf{u} = \sigma - \mu \, \mathbf{sat}(\mathbf{S}) \quad (17)$$

where σ is defined as $-\mathbf{B}_T^{-1}\left(\boldsymbol{D}_{00}\hat{A}_{\mathbf{state}} Y + \dot{f}(\mathbf{Y}_1) \right)$. In order to reduce chattering, the saturation function, **sat** $(\cdot)$, can be replaced by a tangent hyperbolic function. Substituting

$$\mathbf{Y} = \left\{ \begin{matrix} \mathbf{Y}_1 \\ \mathbf{Y}_2 \end{matrix} \right\} = \mathbf{D}\mathbf{X} \left(= \begin{bmatrix} \mathbf{D}_1 \\ \mathbf{D}_2 \end{bmatrix} \mathbf{X} \right)$$

and $\mathbf{Y}_1 = \mathbf{D}_1\mathbf{X}$ in equation (8), the performance index, L_{OPC}, is rearranged as

$$L_{\text{OPC}} = \int_0^\infty \left(\mathbf{X}^{\mathbf{T}}\mathbf{D}^{\mathbf{T}} \begin{bmatrix} \boldsymbol{Q}_{11} & 0 \\ 0 & \boldsymbol{Q}_{22} \end{bmatrix} \mathbf{D}\mathbf{X} \right.$$
$$\left. + \left(\mathbf{X}^{\mathbf{T}}\mathbf{D}_1^{\mathbf{T}} M \mathbf{D}_1\mathbf{X} \right)\left(\mathbf{X}^{\mathbf{T}}\mathbf{D}_1^{\mathbf{T}} \boldsymbol{Q}_{33} \mathbf{D}_1\mathbf{X} \right) + \bar{h}(\mathbf{D}_1\mathbf{X}) \right)\mathrm{d}t \quad (18)$$

which demonstrates the new optimization problem. Comparing equation (18) to equation (4), the matrix, $\mathbf{Q}_1$, and HOT are defined as

$$\mathbf{Q}_1 = \mathbf{D}^{\mathbf{T}} \begin{bmatrix} \boldsymbol{Q}_{11} & 0 \\ 0 & \boldsymbol{Q}_{22} \end{bmatrix} \mathbf{D}$$

$$\text{HOT} = \left(\mathbf{X}^{\mathbf{T}}\mathbf{D}_1^{\mathbf{T}} M \mathbf{D}_1\mathbf{X} \right)\left(\mathbf{X}^{\mathbf{T}} \boldsymbol{Q}_2 \mathbf{X} \right) + \bar{h}(\mathbf{D}_1\mathbf{X}) \, \& \, \mathbf{Q}_2 = \mathbf{D}_1^{\mathbf{T}} \boldsymbol{Q}_{33}\mathbf{D}_1 \quad (19)$$

3. Case study bridge system

The proposed control methodology is applied to a three-span bridge equipped with two semi-active MR dampers attached between adjacent spans. The bridge model includes three reinforced concrete decks, each supported by four rubber bearings, as shown in Figure 1(a). The dimensions of the bridge are given in the longitudinal and top views in Figure 1(b). In this setting, the four supports of span A and the two left supports of span B are positioned on shake-table A, whereas the two right supports of span B and the supports of span C are placed on shake-table B. Considering the short distance between the supports, it is assumed that the ground motions are fully correlated meaning that the same ground motion records are applied to both shake-tables. As the structure is symmetric with respect to the longitudinal axis and ground motions are applied in the longitudinal direction, a one directional model will be able to predict the dynamic response of the decks.

In cases of large deformations, pounding in the bridge may occur between adjacent spans and between spans and abutments. Pounding can be detected by large acceleration spikes in the response of the spans. For seismic pounding mitigation, MR dampers manufactured by Lord Corporation, USA, are installed between adjacent spans for the passively and semi-actively controlled bridge, as shown in Figure 1(a) and Figure 1(b). The input current to the MR dampers which control the forces applied to the system varies from 0 to 2 A, the force capacity is ± 2000 N, the maximum stroke is ± 27.5 mm, the maximum velocity is 200 mm/sec, the extended length is 208 mm, and the weight is about 1 kg. During the shake-table test of the uncontrolled system, displacement and acceleration responses are measured in real-time using piezoelectric sensors and accelerometers, respectively, as shown in Figure 1(c). In the controlled system, the measured responses are used to estimate the state vector through an observer model. In the following subsections, the modeling approach of the bridge components including rubber and lead-rubber bearings, the semi-active device, and the pounding phenomenon is elaborated.

3.1. Models of hysteretic components

Components such as bearings and MR dampers that dissipate energy can be characterized by their hysteretic behaviors (El-Khoury et al., 2015). In order to capture
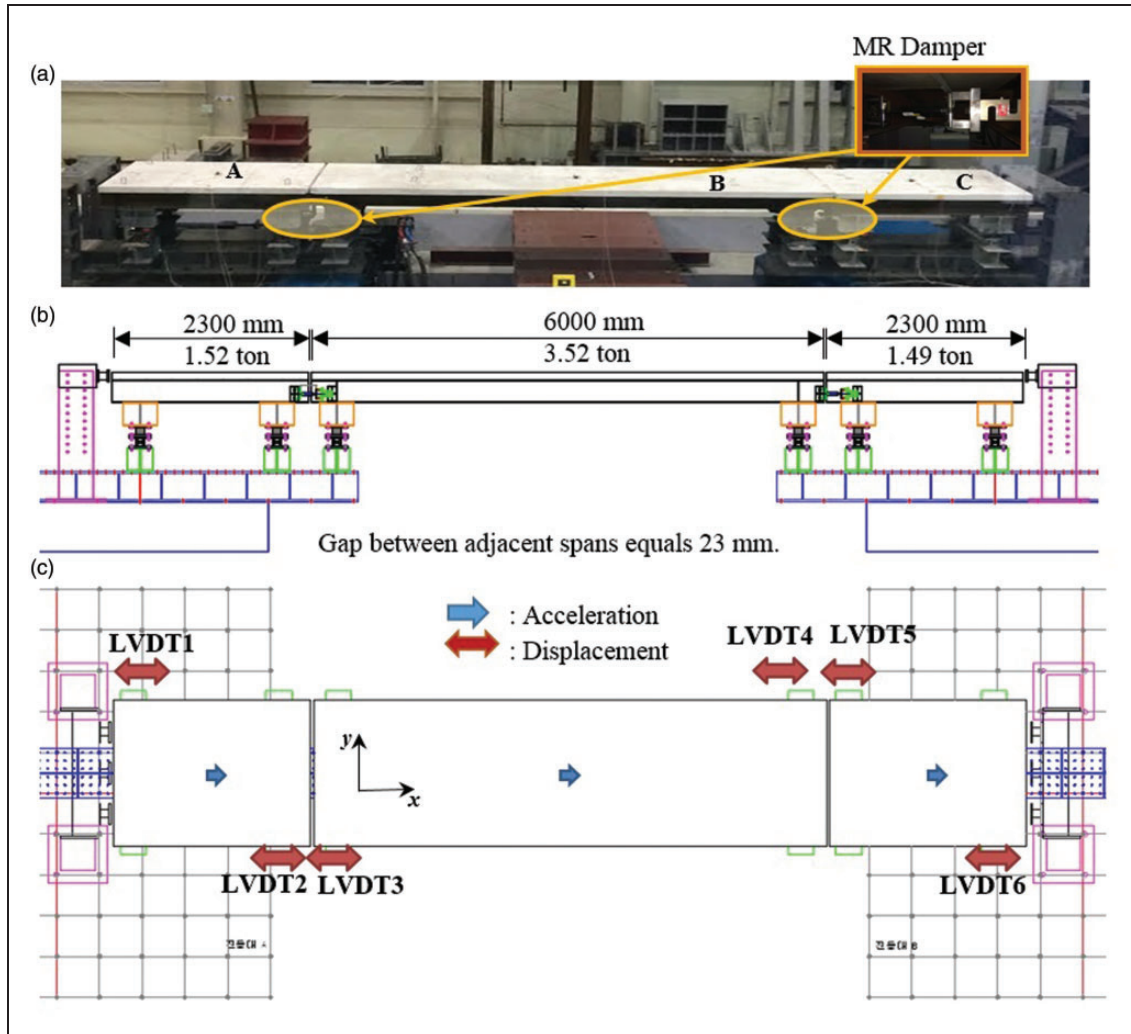
Figure 1. Three-span bridge equipped with magnetorheological (MR) dampers between adjacent spans: (a) a picture of the bridge model taken during shake-table tests, (b) profile view of the three-span bridge, and (c) top view of the three-span bridge indicating the location and direction of linear variable differential transformers (LVDT) and accelerometers.

this type of nonlinearity, the Bouc–Wen model (Bouc, 1971; Wen, 1976) has been extensively used for different applications, for example, system identification of MR dampers (Kwok et al., 2007; Ikhouane and Dyke, 2007), structural elements (Ikhouane et al., 2007), base-isolation devices (Marano et al., 2007), soil material (Gerolymos and Gazetas, 2007), and energy dissipation systems (Shih and Sung, 2005). The hysteresis is a form of nonlinearity where the restoring force depends on both the current deformation and the deformation history (Ikhouane and Rodellar, 2007). Here, the hysteretic force is modeled by a set of stiffness, damping, and hysteresis components, as shown in Figure 2(a). This approach is implemented in this study to represent the nonlinear dynamic behavior of the uncontrolled and controlled bridge. In the uncontrolled state, each span is separated by a gap distance as defined in Figure 2. For the controlled state, the MR damper is

added and modelled by a parallel system of damping, stiffness, and hysteresis, as depicted in Figure 2(b).

To capture the nonlinear behavior of the bearings and the MR damper, the restoring force for the rubber bearing, F_j, and the MR damper, F_{MR}, are modeled as

$$F_j = k_j\big(\alpha_j x_j + \big(1 - \alpha_j\big)z_j\big) \ (j = 1, \ 2, \ 3) \qquad (20)$$

$$F_{MR} = \alpha_{\dot{x}_{MR}}\dot{x}_j + \alpha_{z_{MR}}z_j \ (j = 4, \ 5) \qquad (21)$$

$$\dot{x}_j = \dot{x}_{j-2} - \dot{x}_{j-3}$$

where x_j and $\dot{x}_j$ are the displacement and velocities of jth hysteretic component, respectively. The subscript j ranges from 1 to 5, referring to spans A, B, C, and the MR damper between spans A and B, and between spans B and C. The model parameters k_j, $\alpha_{\dot{x}_{MR}}$, and
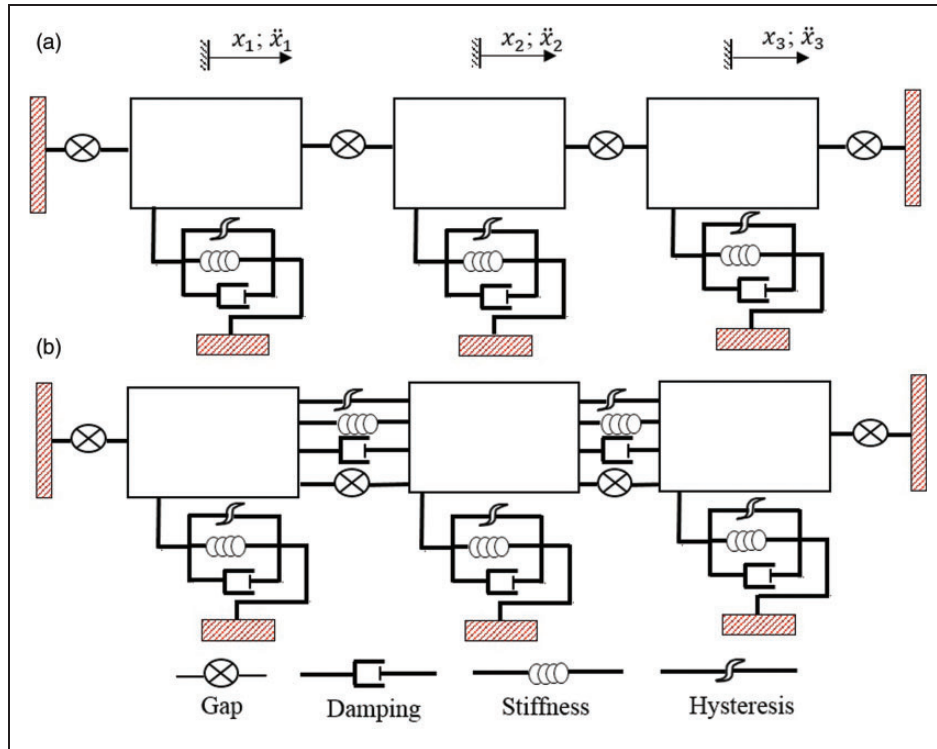
Figure 2. Components of the three-span bridge model in (a) uncontrolled state and (b) controlled state equipped with magnetorheological (MR) dampers.

$\alpha_{z_{MR}}$ are the stiffness and pre-yield factor of rubber bearing, and the damping and hysteretic component of the MR damper, respectively. In addition, the variable, z_j, is the jth evolutionary term governed by the Bouc–Wen differential equation defined as

$$\dot{z}_j = A_j \dot{x}_j - \beta_j |\dot{x}_j| z_j - \gamma_j \dot{x}_j |z_j| \ (j = 1, \ldots 5) \quad (22)$$

where A_j, γ_j, and β_j are parameters that control the shape of the loop. The general slope is controlled by $(\gamma_j + \beta_j)$. Parameters $\alpha_{\dot{x}_{MR}}$ and $\alpha_{z_{MR}}$ are decomposed into passive-off and passive-on components with respect to the current, i_c, as

$$\alpha_{\dot{x}_{MR}} = \alpha_{\dot{x}_{MR}}0 + i_c \alpha_{\dot{x}_{MR}}1 + i_c^2 \alpha_{\dot{x}_{MR}}2 \quad (23)$$

$$\alpha_{z_{MR}} = \alpha_{z_{MR}}0 + i_c \alpha_{z_{MR}}1 + i_c^2 \alpha_{z_{MR}}2 \quad (24)$$

where $\alpha_{\dot{x}_{MR_0}}$, $\alpha_{z_{MR_0}}$, $\alpha_{\dot{x}_{MR_1}}$, $\alpha_{z_{MR_1}}$, $\alpha_{\dot{x}_{MR_2}}$, and $\alpha_{z_{MR_2}}$ and characterize the impact of control current.

To determine the model parameters shown above, a global optimization method based on gradient descent for bearings and MR dampers is used to minimize an error cost function between the experimental data and simulation results (El-Khoury et al., 2015). For the bearings, the three-span bridge is subjected to a scaled Kobe earthquake. The parameters of the nonlinear model for rubber bearings in spans A, B, and C are

Table 1. Calibration results for Bouc–Wen model of rubber bearings.

Rubber bearings					
	Parameters				
Span	A_j	γ_j	β_j	α_j	k_j (N/mm)
A ($j=1$)	1.20	0.26	0.74	0.63	1548.0
B ($j=2$)	1.99	0.89	0.11	0.68	945.2
C ($j=3$)	8.29	0.36	0.64	0.94	1298.0

shown in Table 1. For the MR damper, data of cyclic tests with a frequency of 1 Hz for currents ranging between 0 and 2 A was provided by the manufacturing company. The Bouc–Wen parameters for MR damper are represented as a function of the input current ($\alpha_{\dot{x}_{MR_2}} = -5.7$ N s/mm A^2, $\alpha_{z_{MR_2}} = -10.3$ N/mm.A^2, $\alpha_{\dot{x}_{MR_1}} = 13.1$ N s/mm A, $\alpha_{z_{MR_1}} = 51.9$ N/mm A, $\alpha_{\dot{x}_{MR_0}} = 1.4$ N s/mm, $\alpha_{z_{MR_0}} = 7.0$ N/mm, $A_4 = 45.48$, $\gamma_4 = 0.56$, $\beta_4 = 1.38$). Calibration results are shown in Figure 3 where a good agreement is observed between simulation and experiment results for the MR damper operating at different current levels (0 to 2 A). The force in the MR damper increases with current, from about 250 N at 0 A to around 2000 N at 2 A.
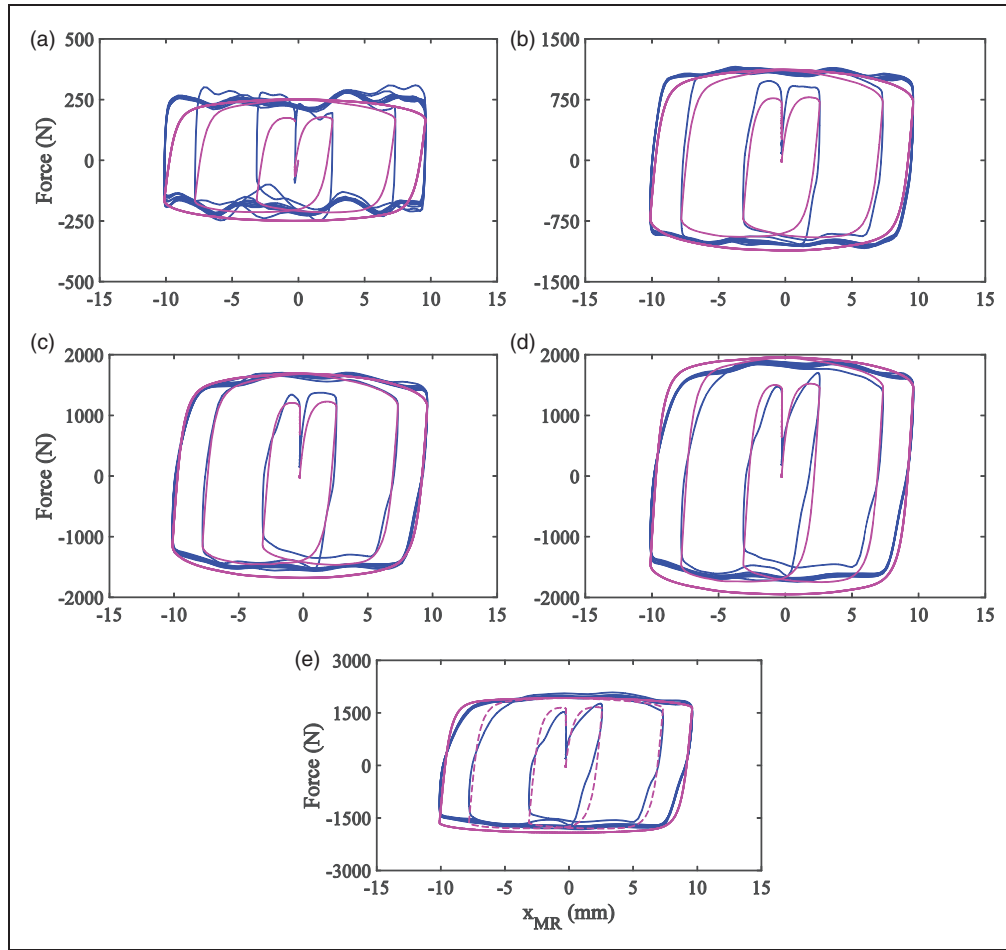
Figure 3. Calibration results based on harmonic tests of the magnetorheological (MR) damper set at different currents: (a) 0.0 A, (b) 0.5 A, (c) 1.0 A, (d) 1.5 A, and 2 A (⎯⎯ Experiment, ⎯⎯ Simulation).

3.2. Pounding model

A damped Hertz impact model is employed here to capture pounding in the bridge when a gap between adjacent segments is closed. According to this model, the impact force can be determined from

$$F_{impact} = k_h \big(\Delta y_{12} - g_p\big)^{\vartheta} \left[1 + \frac{3}{4}\frac{(1-e^2)}{\Delta v_{12}}\dot{y}_{12} \right] \quad (25)$$

where the coefficient of restitution, e, is 0.6 for concrete, k_h is the impact stiffness, g_p is the gap distance, ϑ is the Hertz coefficient that is typically taken as 1.5. The variables, y_{12} and $\dot{y}_{12}$, are the relative displacement and velocity between two adjacent nodes, respectively, while Δv_{12} is the relative velocity before impact (Muthukumar and DesRoches, 2006; El-Khoury et al., 2015).

For experimental verification, pounding can be identified when large spikes in the absolute acceleration responses are observed. For instance, if opposite spikes at a given instant are observed in the absolute accelerations of adjacent spans, it indicates that pounding has occurred between those spans. Elsewhere, a large spike in the total span acceleration is an indication of the pounding between that span and the adjacent abutment. The pounding model is tested for the uncontrolled three-span bridge subjected to KB40 and the response is plotted in Figure 4. It can be observed that pounding occurred primarily between adjacent spans. In addition, the pounding model was able to capture the majority of acceleration spikes.

4. Implementation of the control algorithm

As mentioned earlier, this paper investigates the semi-active control of a nonlinear partially observed system. In order to achieve an optimal control performance, a number of additional steps are taken in the control design including linearization of the system, modeling constraints of the semi-active control force,
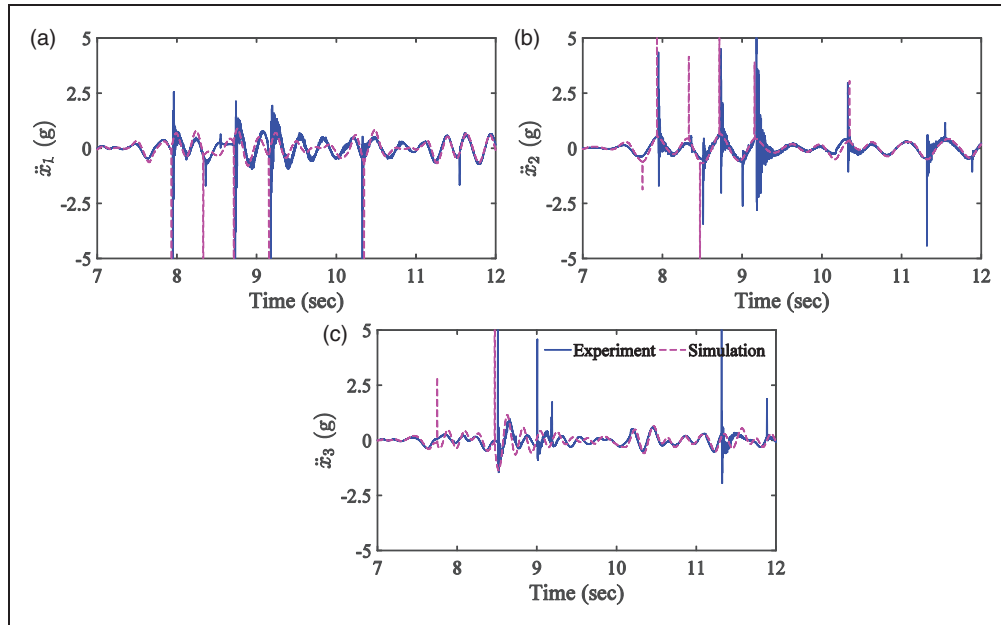
Figure 4. Acceleration response of the three-span bridge subjected to KB40: (a) span A, (b) span B, and (c) span C.

and designing an observer for the partially observed system. First, the nonlinear passive-off bridge model is linearized stochastically. Next, a second-level optimization is carried out in order to find the optimal gains of the SMC-OPC controller such that the performance of the MR damper is maximized based on a defined objective function. A clipped optimal strategy and a Kalman-based observer are designed to drive the MR damper forces into a feasible range based on current saturation and to estimate the state space given the measured responses, respectively.

4.1. Stochastic linearization

In conventional linearization, the nonlinearity of the components is ignored and the system is calibrated and linearized based on initial or equivalent linear stiffness, which may yield inaccurate response predictions. Stochastic linearization replaces the hysteretic components by equivalent linear time invariant models through minimizing the residual errors arising from the linearization process (Basili and De Angelis, 2007; Basili et al., 2013; El-Khoury et al., 2015). The stochastic linearization strategy is applied to the three-span bridge equipped with MR dampers at zero current. The equation of motion of the dynamic system is presented as

$$\mathbf{M\ddot{U}} + \mathbf{C_d\dot{U}} + \mathbf{K_U U} + \mathbf{K_Z Z} = \mathbf{M\ddot{x}_g} \qquad (26)$$

where the matrices, $\mathbf{M}$, $\mathbf{C_d}$, $\mathbf{K_U}$, and $\mathbf{K_Z}$ are the mass, damping, linear stiffness, and nonlinear stiffness matrices, respectively. $\mathbf{U}$ is the linear displacement vector identified as $[x_1; x_2; x_3]$, and $\mathbf{Z}$ is the evolutionary vector presented as $[z_1; z_2; z_3; z_4; z_5]$. The variables x_1, x_2, x_3 are displacements of spans A, B and C, and z_1, z_2, z_3, z_4, and z_5 are the hysteretic terms in the support models for spans A, B, and C, and the two MR dampers, respectively. $\mathbf{\ddot{x}_g}$ is the ground motion vector applied to the three-span bridge. As mentioned in Section 3.1, the hysteretic behavior is characterized by the Bouc–Wen model, presented as

$$\dot{z}_j = \mathrm{A}\dot{x}_j - \beta|\dot{x}_j|z_j - \gamma\dot{x}_j|z_j| \qquad (27)$$

where the subscript, j ($=1, 2\dots 5$), refers to spans A, B, and C, and MR dampers, respectively. Since this equation depends only on the velocity and hysteretic term, the equivalent linearized equation is presented as

$$\dot{z}_j = -\mathrm{C}_j\dot{x}_j - \mathrm{K}_j z_j \qquad (28)$$

where C_j and K_j are the linearized parameters of the velocity and hysteretic term, respectively. Under the assumption that $\dot{x}_j$ and z_j are zero mean joint Gaussian processes, the linearized parameters, C_j and K_j, are obtained by partially differentiating equation (28) with respect to $\dot{x}_j$ and z_j, respectively:

$$\mathrm{C}_j = -\frac{\partial(\dot{z}_j)}{\partial(\dot{x}_j)}, \mathrm{K}_j = -\frac{\partial(\dot{z}_j)}{\partial(z_j)} \qquad (29)$$

Applying equation (28) to equation (26), the linearized parameters are presented as

$$C_j = \beta_j E\left[\frac{z\partial(|\dot{x}_j|)}{\partial \dot{x}_j}\right] + \gamma_j E[|z_j|] - A_j \quad (30)$$

$$K_j = \beta_j E[|\dot{x}_j|] + \gamma_j E\left[\frac{\dot{x}_j\partial(|z_j|)}{\partial z_j}\right] \quad (31)$$

Since the external excitation is assumed to be a Gaussian process and the variables are jointly Gaussian, the linearized parameters can be evaluated in terms of the second moments as follows

$$C_j = \sqrt{\frac{2}{\pi}}\left[\beta_j\sigma_{z_j} + \frac{\gamma_j E(\dot{x}_j z_j)}{\sigma_{\dot{x}_j}}\right] - A_j \quad (32)$$

$$K_j = \sqrt{\frac{2}{\pi}}\left[\frac{\beta_j E(\dot{x}_j z_j)}{\sigma_{z_j}} + \gamma_j\sigma_{\dot{x}_j}\right] \quad (33)$$

where $E(\dot{x}_j z_j)$ is the expected value of $\dot{x}_j z_j$, and $\sigma_{\dot{x}_j}^2$ and $\sigma_{z_j}^2$ are the variances of $\dot{x}_j$ and z_j, respectively (Socha 2008; To, 2011). Using the initial values of the linearized parameters, a Lyapunov equation is used to compute the second moments which are then substituted in equations (32) and (33) until the difference in the results of the pth and $(p+1)$th iterations is within a prescribed margin of error. Next, the converged linearized parameters, C_j and K_j are substituted in equation (28) and rearranged in the state space. Consequently, the linearized bridge model is derived as

$$\dot{X} = A_{state}X + F_e \quad (34)$$

where the state vector, X, is defined as

$$X = [U; \dot{U}; Z] \quad (35)$$

The system matrix, A_{state}, includes mass, damping, and nonlinear stiffness components of the three-span bridge:

$$A_{state} = \begin{bmatrix} 0 & I & 0 \\ -M^{-1}K_U & -M^{-1}C_d & -M^{-1}K_Z \\ 0 & C_b & K_b \end{bmatrix} \quad (36)$$

where C_b, K_b, and F_e are the linearized parameters for velocity and hysteretic components in the system and the external excitation vector, respectively. This procedure is used to derive the stochastic linear model of the passive-controlled system, i.e. the bridge model combined with the passive component of the MR damper. The performance of this model is compared to the nonlinear and linear elastic models of the bridge for the Kobe ground motion scaled at 40% (KB40), and the results are presented in Figure 5. It is seen that the stochastically linearized model predicts well the response of the nonlinear bridge compared to the deterministic linear elastic model. This performance is expected since stochastic linearization replaces the nonlinear differential equation of the system by a linear one that is derived based on statistical measures considering the hysteretic behavior of the bridge. This ensures more accurate representation of system responses compared to the conventional linear elastic approach, which ignores the z component.
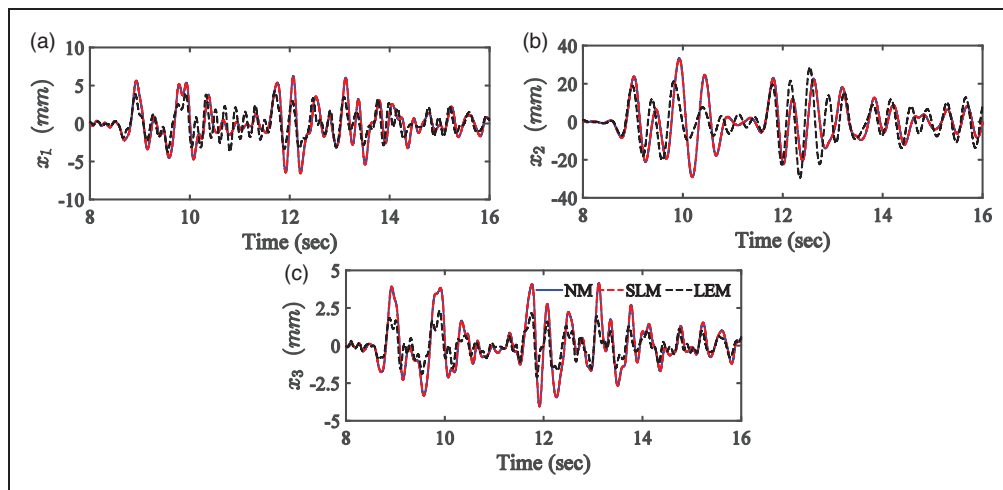
Figure 5. Time history of nonlinear model (NM) versus stochastic linearization (SLM) and linear elastic linearization (LEM) methods for (a) displacement of span A, (b) displacement of span B, and (c) displacement of span C under KB40.

4.2. Second-level optimization

The weighting matrices in equations (18) and (19) are commonly determined based on the designer's prior knowledge or an iterative procedure. However, such methods may not yield optimal results in most cases and better solutions can be achieved through a well-defined second-level optimization. In order to determine the optimal weighting matrices, Q_1 and Q_2, and the parameter, μ, in equations (17), (18), and (19), a second-level optimization cost function can be defined based on the interest and the judgment of the designer.

$$\boldsymbol{u}_{\text{constrained}} = \begin{bmatrix} u_{\text{constrained}_1} \\ u_{\text{constrained}_2} \end{bmatrix} = \begin{bmatrix} 0 & \Delta_j < 0\,\text{Amp} \\ u_{\text{unconstrained}_{j-3}} & 0\,\text{Amp} \leq \Delta_j \leq 2\,\text{Amp} \\ -\left(2\alpha_{\dot{x}_{\text{MR}_1}} + 2^2\alpha_{\dot{x}_{\text{MR}_2}}\right)\dot{x}_j + \left(2\alpha_{z_{\text{MR}_1}} + 2^2\alpha_{z_{\text{MR}_2}}\right)z_j & \Delta_j > 2\,\text{Amp} \end{bmatrix}_{j-3} \quad (38)$$

Here, the second-level global optimization problem is defined by a cost function which includes a combination of different response variables. For the three-span bridge, one of the primary objectives of the control strategy is to reduce the likelihood of pounding and acceleration. To consider a combination of the critical responses, an objective function, L$_2$, is considered to incorporate the critical displacements (pounding) and absolute span accelerations:

$$L_2 = \left(\frac{\max^-_{x_1 C}}{\max^-_{x_1 P}} + \frac{\max^+_{x_{12} C}}{\max^+_{x_{12} P}} + \frac{\max^+_{x_{23} C}}{\max^+_{x_{23} P}} + \frac{\max^+_{x_3 C}}{\max^+_{x_3 P}} \right. $$
$$\left. + \frac{\max_{\ddot{x}_1 C}}{\max_{\ddot{x}_1 P}} + \frac{\max_{\ddot{x}_2 C}}{\max_{\ddot{x}_2 P}} + \frac{\max_{\ddot{x}_3 C}}{\max_{\ddot{x}_3 P}} \right)_{[\mathbf{Q}_1, \mathbf{Q}_2, \mu]} \quad (37)$$

where the subscripts $(\cdot)_C$ and $(\cdot)_P$ refer to the SMC-OPC and passive-on states, respectively. The critical displacements are relative displacements between two sides of a gap in the direction of gap closure. For example, $\max^+_{x_{12} C}$ refers to the maximum of the positive relative displacement of span A with respect to span B, while $\max^-_{x_1 C}$ represents the maximum relative displacement of span C with respect to the adjacent abutment in the negative direction. If these displacements are equal to the corresponding gap sizes, pounding will occur. On the other hand, $\max_{12_C}$ refers to the maximum absolute relative displacement of span A and span B irrespective of direction; that is, $\max(|x_1 - x_2|)$. The first four components consider the ratio of the max directional displacements, whereas the rest of the components take into account the ratio of the maximum absolute acceleration responses in the semi-actively controlled versus passively controlled bridge.

4.3. Clipped semi-active control forces

During simulation and shake-table tests, clipped optimal rules are considered in order to apply the control force constraints of the semi-active device. These constraints include the dependency of the applied control force on the direction of the dynamic response of the MR damper and the force capacity of the device. To incorporate these limitations in the control model, the feasible range of 0 and 2 A for the input current to the MR damper is considered and the following force saturation model is applied.

where $\Delta_j (j = 4, 5)$ is the root of

$$u_{\text{unconstrained}_j} - \left(\Delta_j \alpha_{\dot{x}_{\text{MR}_1}} + \Delta_j^2 \alpha_{\dot{x}_{\text{MR}_2}}\right)\dot{x}_j$$
$$+ \left(\Delta_j \alpha_{z_{\text{MR}_1}} + \Delta_j^2 \alpha_{z_{\text{MR}_2}}\right)z_j = 0 \quad (39)$$

and the unconstrained control force vector, $\boldsymbol{u}_{\text{unconstrained}}$, is the active control force from equation (17).

5. Results

In order to evaluate the control performance of the three-span bridge subjected to seismic excitations, four cases are considered for shake-table experiments:

(a) uncontrolled, where no MR damper is installed on the bridge;
(b) passive-off, where two MR dampers are installed between adjacent spans and are set to minimum current of 0 A;
(c) passive-on, where both dampers are set to maximum current of 2 A;
(d) SMC-OPC control, where a current value is determined from the control algorithm and fed into the MR damper instantaneously.

In this study, the Kobe earthquake is considered, which is a near-field event with high-amplitude, long-period velocity pulses and a peak ground acceleration (PGA) of 0.821 g. This ground motion exported from NGA database (Chiou and Youngs, 2008) was recorded at the KJMA Observatory station, with a distance to fault rupture of 0.6 km.
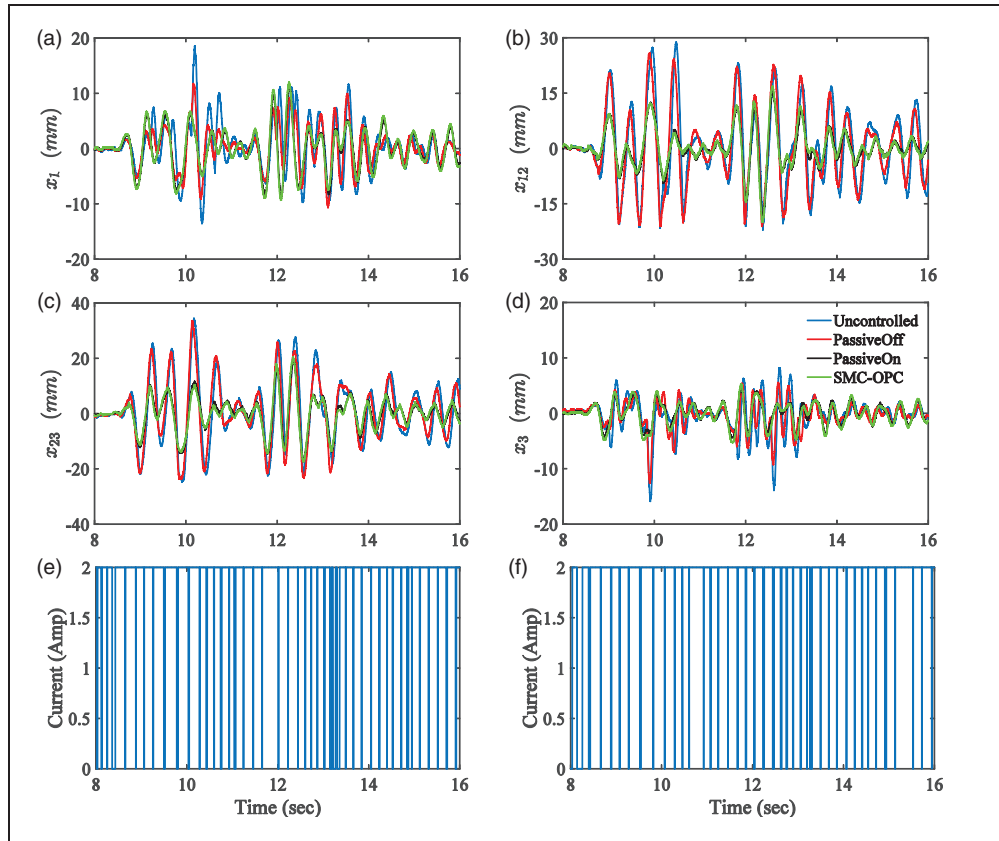
Figure 6. Time history response of the three-span bridge with various control states subjected to KB40 for displacements of (a) span A, (b) AB, (c) BC, and (d) span C and current of magnetorheological (MR) dampers (e) AB and (f) BC. SMC-OPC: sliding mode control-optimal polynomial control.

The results, here, are analyzed for Kobe ground motion scaled at 20% (KB20) and 40% (KB40). For KB20, no pounding is observed in any of the cases; however, the critical displacement responses, x_{12}^+ and x_{23}^+, are reduced to 23% and 48% at passive-on state and 28% and 61% at semi-active state, respectively, in comparison to the uncontrolled case. As for the acceleration responses, the passive-off case has the smallest absolute accelerations, in which $\ddot{x}_1$, $\ddot{x}_2$, and $\ddot{x}_3$ are reduced by 10%, 13%, and 1%, respectively, compared to the uncontrolled case.

For KB40, the performance of passive and semi-active control strategies are more pronounced as compared to the uncontrolled bridge. For this scaled ground motion, significant pounding is observed between adjacent spans in both the uncontrolled and passive-off states. Nevertheless, the number of acceleration spikes for passive-off are reduced by at least 25% compared to the uncontrolled state; four spikes for $\ddot{x}_1$, eight spikes for $\ddot{x}_2$, and four spikes for $\ddot{x}_3$. As for the semi-actively controlled system, a significant improvement is shown compared to the uncontrolled state especially where 41% and 32% reductions in the relative displacements, x_{12} and x_{23} are observed. For the same

response measures, these reductions are 46% and 37% for the passive-on control case. For further illustration, the time history of displacement and acceleration responses are shown in Figures 6 and 7. In addition, the bearing forces applied on span B are plotted in Figure 8 where a pronounced improvement is observed in terms of the peak forces compared to the uncontrolled case: 32% reduction for both passive-on and SMC-OPC, and 13% reduction for passive-off. Similar behaviors are seen for bearings of spans A and C.

One of the main advantages of the control algorithm is its performance convergence to that of passive-on but at a lower cost by minimizing current and energy consumptions, as recorded in Tables 2 and 3. The control energy, E, of an MR damper is a more accurate measure than current to indicate the power consumption of the system. The control energy is defined as

$$E = i^2 R_{\text{coil}} \qquad (40)$$

where R_{coil} is the resistance of the coil wire (Nguyen et al., 2008). The results can be summarized as follows: the mean current values for semi-active MR-AB and
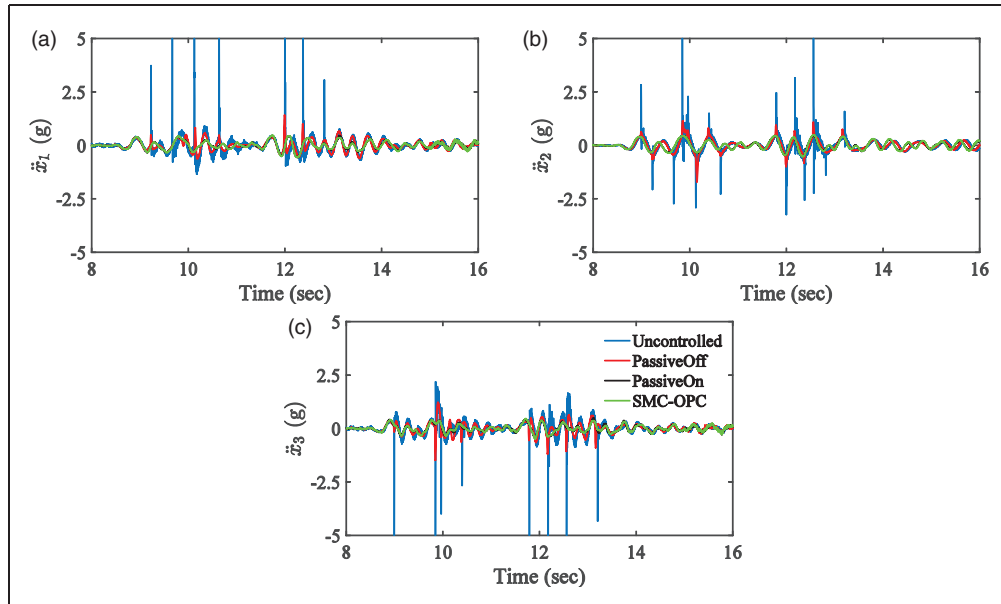
Figure 7. Absolute acceleration time history of three-span bridge for different control states subjected to KB40 for (a) span A, (b) span B, and (c) span C. SMC-OPC: sliding mode control-optimal polynomial control.
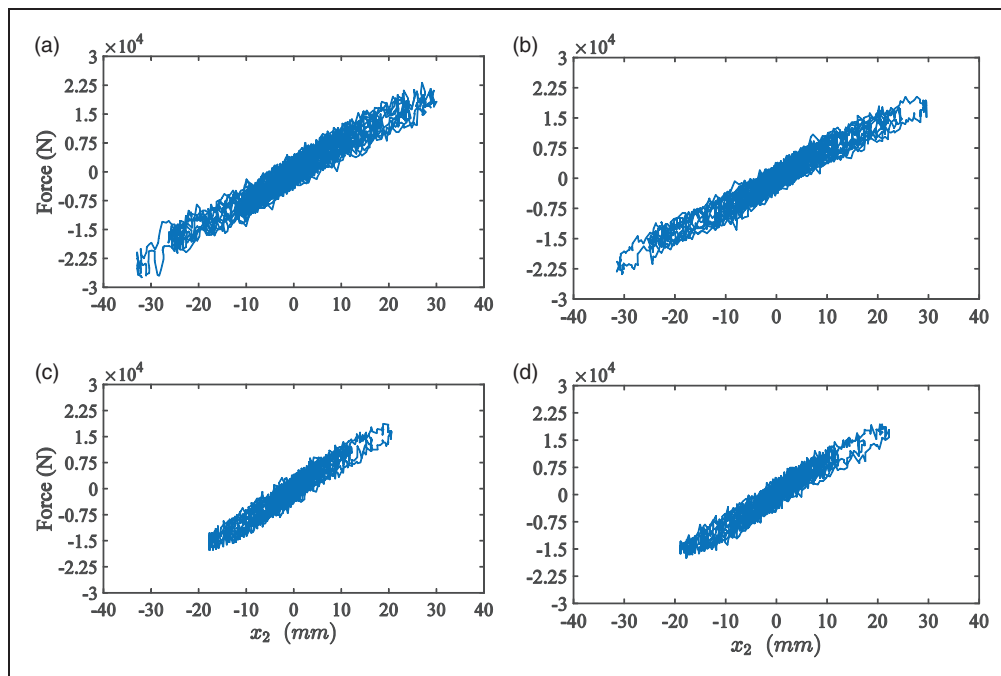
Figure 8. Force–deformation behavior of bearing forces applied to span B under KB40 for (a) uncontrolled, (b) passive-off, (c) passive-on, and (d) SMC-OPC (sliding mode control-optimal polynomial control).

MR-BC at KB40 are reduced to 74% and 53% of passive-on case, and the energy consumptions for both MR dampers are reduced further to 37% and 26% of passive-on state. Similar results are observed for KB20, where the power consumption is reduced by 69% for both MR dampers compared to passive-on case.

From the experiment results especially for the high-intensity earthquake, it appears that reducing critical displacements helps in avoiding pounding and hence the acceleration values stay within moderate levels. Adding MR dampers enhances the energy dissipation capabilities of the system especially for ground motions

Table 2. Results for three-span bridge subjected to KB20.

	Critical/Peak displacements (mm) and peak accelerations (g)						
State	x_1	x_{12}	x_{23}	x_3	$\ddot{x}_1$	$\ddot{x}_2$	$\ddot{x}_3$
Uncontrolled	2.40/2.80	16.61/17.05	16.50/17.10	1.32/1.64	0.33	0.38	0.27
Passive-off	2.75/2.65	12.34/12.34	11.56/12.61	1.41/1.83	0.30	0.33	0.27
Passive-on	4.93/6.01	3.89/6.01	8.04/8.04	3.20/3.36	0.36	0.35	0.30
SMC-OPC	4.76/6.3	4.64/7.15	10.01/10.11	2.92/3.08	0.33	0.35	0.36

	RMS of displacements (mm) and accelerations (g)						
State	x_1	x_{12}	x_{23}	x_3	$\ddot{x}_1$	$\ddot{x}_2$	$\ddot{x}_3$
Uncontrolled	0.32	2.42	2.43	0.23	0.05	0.06	0.04
Passive-off	0.37	1.78	1.79	0.26	0.05	0.05	0.04
Passive-on	0.65	0.50	0.70	0.78	0.05	0.05	0.05
SMC-OPC	0.69	0.66	0.82	0.865	0.05	0.05	0.05

Current Ratio $= \dfrac{\bar{i}_{SMC-OPC}}{\bar{i}_{Passive-on}}$ / Energy Ratio $= \dfrac{\bar{E}_{SMC-OPC}}{\bar{E}_{Passive-on}}$

State	MR-AB	MR-BC
SMC-OPC	0.61 / 0.31	0.62 / 0.31

Table 3. Results for three-span bridge subjected to KB40.

	Critical/Peak displacements (mm) and peak accelerations (g)						
State	x_1	x_{12}	x_{23}	x_3	$\ddot{x}_1$	$\ddot{x}_2$	$\ddot{x}_3$
Uncontrolled	13.62/18.56	28.88/28.88	30.31/30.31	8.24/15.95	7.32	7.60	16.79
Passive-off	10.73/11.79	25.99/25.99	29.00/29.00	4.38/12.66	5.52	4.09	11.28
Passive-on	8.72/11.22	15.70/18.94	19.49/19.49	4.87/4.76	0.59	0.53	0.51
SMC-OPC	9.37/11.99	16.97/19.97	20.48/20.48	5.32/5.52	0.62	0.55	0.53

	RMS of displacements (mm) and accelerations (g)						
State	x_1	x_{12}	x_{23}	x_3	$\ddot{x}_1$	$\ddot{x}_2$	$\ddot{x}_3$
Uncontrolled	1.82	4.23	4.64	4.84	1.26	0.17	0.15
Passive-off	1.42	4.11	4.42	0.80	0.10	0.11	0.10
Passive-on	1.45	1.97	2.38	2.71	0.08	0.08	0.07
SMC-OPC	1.54	2.02	2.35	2.84	0.08	0.09	0.07

Current Ratio $= \dfrac{\bar{i}_{SMC-OPC}}{\bar{i}_{Passive-on}}$ / Energy Ratio $= \dfrac{\bar{E}_{SMC-OPC}}{\bar{E}_{Passive-on}}$

State	MR-AB	MR-BC
SMC-OPC	0.74 / 0.37	0.53 / 0.26

with large PGA. Using these strategies, the likelihood of failure, collapse, and pounding can be noticeably reduced. For semi-active control, the performance of the system converges to that of the passive-on state with a considerable reduction in the energy consumption, as shown earlier. However, if the damper cannot operate semi-actively or at a constant nonzero current value, the passive-off state can still reduce the impact of

pounding as observed with fewer and less severe acceleration spikes compared to uncontrolled state (Figure 7). As a result, both passive and semi-active strategies have noticeable impacts on the seismic performance of the bridge and can be adopted as alternative solutions for seismic risk reduction of critical structures.

6. Conclusion

In this paper, the effectiveness of MR dampers controlled using passive and semi-active strategies are examined for response reduction and in particular pounding mitigation of adjacent structures. The damper is set at zero current, maximum current, and a current value that is determined through a semi-active control strategy. In that respect, a new state-space-based control algorithm, named SMC-OPC is introduced and derived. SMC-OPC is based on a nonlinear sliding mode control, in which the linear sliding surface is expanded to a higher order trajectory. The higher order surface provides more flexibility to optimize the performance and maximize the robustness of the controller compared to linear sliding surfaces. Alongside the passive states, SMC-OPC is designed and tested using shake-table experiments for a three-span bridge supported by nonlinear bearings. For this system, the control objectives are to reduce excessive deformations that may lead to collapse and the potential of pounding, depicted by spikes of absolute accelerations, since it may pose considerable damage to adjacent structures.

To suppress the extreme effects of seismic-induced vibrations, two MR dampers are installed between adjacent spans. For semi-active technology, the clipped semi-active control strategy is adopted to optimize the performance of the MR damper as compared to the three conditions: uncontrolled, passive-off where the input current is zero, and passive-on which has the maximum input current of 2 A. The control design process starts with developing numerical models for the characterization of nonlinear components of the system. The hysteresis in both the MR damper and rubber bearings is simulated using Bouc–Wen model, whereas the nonlinear pounding phenomenon between spans and abutments is captured using a damped Hertz model.

To design the state-space control strategy, the nonlinear system is stochastically linearized where the nonlinear behavior of the passive MR damper is incorporated. Next, a clipped optimal strategy is utilized to account for MR damper constraints in the SMC-OPC algorithm. To provide an optimal performance of the control device, the selection of the weighting matrices is made based on a global second-level optimization of a prescribed cost function. Shake-table experiments are conducted for the bridge models for scaled near-field ground motion records. The results show that passive-on at the stronger earthquake provides the best control performance with respect to reducing structural responses. The proposed SMC-OPC semi-active control method provides a balance between the performance of the controlled system with respect to its reliability, and the power consumption of the controller which affects the performance of the control device during the event. This strategy yields very close performance to the passive-on case but with significantly reduced energy consumption during the large ground motion. Although the passive-off state is not as efficient as SMC-OPC and passive-on, it is able to noticeably reduce displacement and acceleration responses compared to the uncontrolled state during moderate and large earthquakes. This observation is important as passive-off state can represent the case where the power supply to the MR damper is failed. Considering these factors, it can be concluded that installation of MR dampers between adjacent structures has the potential to reduce damage due to pounding and excessive gap openings in adjacent structures in addition to mitigating other critical structural responses. Such passive and semi-active strategies can keep bridges operational following moderate and large seismic events.

References

Abdel-Rohman M and John MJ (2006) Control of wind-induced nonlinear oscillations in suspension bridges using multiple semi-active tuned mass dampers. *Journal of Vibration and Control* 12: 1011–1046.

Adhikari R and Yamaguchi H (1997) Sliding mode control of buildings with ATMD. *Earthquake Engineering & Structural Dynamics* 26: 409–422.

Agrawal A, Tan P, Nagarajaiah S, et al. (2009) Benchmark structural control problem for a seismically excited highway bridge—Part I: Phase I problem definition. *Structural Control and Health Monitoring* 16: 509–529.

Agrawal AK, Yang JN and He WL (2003) Applications of some semiactive control systems to benchmark cable-stayed bridge. *Journal of Structural Engineering* 129: 884–894.

Andrawes B and DesRoches R (2007) Comparison between shape memory alloy seismic restrainers and other bridge retrofit devices. *Journal of Bridge Engineering* 12: 700–709.

Bajaj HM, Singh Birdi G and Ugale BA (2014) Application of magnetorheological (MR) fluid damper and its social

impact. *International Journal of Mechanical and Production Engineering* 2: 41–45.

Basili M and De Angelis M (2007) Optimal passive control of adjacent structures interconnected with nonlinear hysteretic devices. *Journal of Sound and Vibration* 301: 106–125.

Basili M, De Angelis M and Fraraccio G (2013) Shaking table experimentation on adjacent structures controlled by passive and semi-active MR dampers. *Journal of Sound and Vibration* 332: 3113–3133.

Bouc R (1971) Modèle mathématique d'hystérésis. *Acustica* 24: 16–25.

Chiou BJ and Youngs RR (2008) An NGA model for the average horizontal component of peak ground motion and response spectra. *Earthquake Spectra* 24: 173–215.

DesRoches R, Pfeifer T, Leon RT, et al. (2003) Full-scale tests of seismic cable restrainer retrofits for simply supported bridges. *Journal of Bridge Engineering* 8: 191–198.

DesRoches R, Comerio M, Eberhard M, et al. (2011) Overview of the 2010 Haiti earthquake. *Earthquake Spectra* 27: S1–S21.

Dicleli M and Mansour MY (2003) Seismic retrofitting of highway bridges in Illinois using friction pendulum seismic isolation bearings and modeling procedures. *Engineering Structures* 25: 1139–1156.

El-Khoury O, Kim C, Shafieezadeh A, et al. (2015) Experimental study of the semi-active control of a nonlinear two-span bridge using stochastic optimal polynomial control. *Smart Materials and Structures* 24: 1–15.

Efraimiadou S, Hatzigeorgiou GD and Beskos DE (2013) Structural pounding between adjacent buildings subjected to strong ground motions. Part I: The effect of different structures arrangement. *Earthquake Engineering & Structural Dynamics* 42: 1509–1528.

Fan YC, Loh CH, Yang JN, et al. (2009) Experimental performance evaluation of an equipment isolation using MR dampers. *Earthquake Engineering & Structural Dynamics* 38: 285–305.

Gerolymos N and Gazetas G (2007) A model for grain-crushing-induced landslides: application to Nikawa, Kobe 1995. *Soil Dynamics and Earthquake Engineering* 27: 803–817.

Guclu R (2006) Sliding mode and PID control of a structural system against earthquake. *Mathematical and Computer Modelling* 44: 210–217.

Guo A, Li Z, Li H, et al. (2009) Experimental and analytical study on pounding reduction of base-isolated highway bridges using MR dampers. *Earthquake Engineering & Structural Dynamics* 38: 1307–1333.

Han Q, Du X, Liu J, et al. (2009) Seismic damage of highway bridges during the 2008 Wenchuan earthquake. *Earthquake Engineering and Engineering Vibration* 8: 263–273.

Huo Y and Zhang J (2012) Effects of pounding and skewness on seismic responses of typical multispan highway bridges using the fragility function method. *Journal of Bridge Engineering* 18: 499–515.

Huo L, Song G, Nagarajaiah S, et al. (2012) Semi-active vibration suppression of a space truss structure using a fault tolerant controller. *Journal of Vibration and Control* 18: 1436–1453.

Ikhouane F and Dyke SJ (2007) Modeling and identification of a shear mode magnetorheological damper. *Smart Materials and Structures* 16: 605–616.

Ikhouane F and Rodellar J (2007) *Systems with Hysteresis: Analysis, Identification and Control Using the Bouc-Wen Model*. Chichester: John Wiley & Sons.

Ikhouane F, Mañosa V and Rodellar J (2007) Dynamic properties of the hysteretic Bouc-Wen model. *Systems & Control Letters* 56: 197–205.

Johnson N, Ranf RT, Saiidi MS, et al. (2008) Seismic testing of a two-span reinforced concrete bridge. *Journal of Bridge Engineering* 13: 173–182.

Kawashima K, Takahashi Y, Ge H, et al. (2009) Reconnaissance report on damage of bridges in 2008 Wenchuan, China, earthquake. *Journal of Earthquake Engineering* 13: 965–996.

Kim SH and Shinozuka M (2004) Development of fragility curves of bridges retrofitted by column jacketing. *Probabilistic Engineering Mechanics* 19: 105–112.

Kim SJ, Holub CJ and Elnashai AS (2010) Analytical assessment of the effect of vertical earthquake motion on RC bridge piers. *Journal of Structural Engineering* 137: 252–260.

Kwok NM, Ha QP, Nguyen MT, et al. (2007) Bouc–Wen model parameter identification for a MR fluid damper using computationally efficient GA. *ISA Transactions* 46: 167–179.

Kwon HC, Kim MC and Lee IW (1998) Vibration control of bridges under moving loads. *Computers & Structures* 66: 473–480.

Leavitt J, Bobrow JE, Jabbari F, et al. (2006) Application of a high-pressure gas semi-active resettable damper to the benchmark smart base-isolated building. *Structural Control and Health Monitoring* 13: 748–757.

Lee TY and Chen PC (2011a) Experimental and analytical study of sliding mode control for isolated bridges with MR dampers. *Journal of Earthquake Engineering* 15: 564–581.

Lee TY and Chen PC (2011b) Sliding mode control for nonlinear isolated bridges. *Journal of Earthquake Engineering* 15: 582–600.

Maddaloni G, Caterino N and Occhiuzzi A (2011) Semi-active control of the benchmark highway bridge based on seismic early warning systems. *Bulletin of Earthquake Engineering* 9: 1703–1715.

Marano GC, Greco R, Trentadue F, et al. (2007) Constrained reliability-based optimization of linear tuned mass dampers for seismic control. *International Journal of Solids and Structures* 44: 7370–7388.

Moustafa MA and Mosalam KM (2015) Seismic response of bent caps in as-built and retrofitted reinforced concrete box-girder bridges. *Engineering Structures* 98: 59–73.

Muthukumar S and DesRoches R (2006) A Hertz contact model with non-linear damping for pounding simulation. *Earthquake Engineering & Structural Dynamics* 35: 811–828.

Naserkhaki S, Aziz FNA and Pourmohammad H (2012) Earthquake induced pounding between adjacent buildings considering soil-structure interaction. *Earthquake Engineering and Engineering Vibration* 11: 343–358.

Nguyen QH, Choi SB and Wereley NM (2008) Optimal design of magnetorheological valves via a finite element method considering control energy and a time constant. *Smart Materials and Structures* 17: 1–12.

Ni YQ, Spencer BF and Ko JM (2001) Feasibility of active control of cable-stayed bridges: an insight into Ting Kau Bridge. In: *SPIE's 8th annual international symposium on smart structures and materials*, July 2001, pp.387–398. Newport Beach, CA, USA: International Society for Optics and Photonics.

Padgett JE, DesRoches R and Ehlinger R (2010) Experimental response modification of a four-span bridge retrofit with shape memory alloys. *Structural Control and Health Monitoring* 17: 694–708.

Pamuk A, Kalkan E and Ling HI (2005) Structural and geotechnical impacts of surface rupture on highway structures during recent earthquakes in Turkey. *Soil Dynamics and Earthquake Engineering* 25: 581–589.

Park KS, Koh HM, Ok SY, et al. (2005) Fuzzy supervisory control of earthquake-excited cable-stayed bridges. *Engineering Structures* 27: 1086–1100.

Raheem SEA (2009) Pounding mitigation and unseating prevention at expansion joints of isolated multi-span bridges. *Engineering Structures* 31: 2345–2356.

Saaed TE, Nikolakopoulos G, Jonasson J, et al. (2015) A state-of-the-art review of structural control systems. *Journal of Vibration and Control* 21: 919–937.

Saiidi MS, Vosooghi A and Nelson RB (2012) Shake-table studies of a four-span reinforced concrete bridge. *Journal of Structural Engineering* 139: 1352–1361.

Shih MH and Sung WP (2005) A model for hysteretic behavior of rhombic low yield strength steel added damping and stiffness. *Computers & Structures* 83: 895–908.

Socha L (2008) *Linearization Methods for Stochastic Dynamic Systems*. Springer Science & Business Media.

Song WK and Kim SE (2007) Analysis of the overall collapse mechanism of cable-stayed bridges with different cable layouts. *Engineering Structures* 29: 2133–2142.

To CW (2011) *Nonlinear Random Vibration: Analytical Techniques and Applications*. Boca Raton, FL: CRC Press.

Utkin VI (1992) *Sliding Modes in Control and Optimization*. Berlin: Springer-Verlag.

Wang AP and Lin YH (2007) Vibration control of a tall building subjected to earthquake excitation. *Journal of Sound and Vibration* 299: 757–773.

Wen YK (1976) Method for random vibration of hysteretic systems. *Journal of the engineering mechanics division* 102: 249–263.

Won JH, Mha HS and Kim SH (2015) Effects of the earthquake-induced pounding upon pier motions in the multi-span simply supported steel girder bridge. *Engineering Structures* 93: 1–12.

Yang MG and Cai CS (2015) Longitudinal vibration control for a suspension bridge subjected to vehicle braking forces and earthquake excitations based on magnetorheological dampers. *Journal of Vibration and Control* DOI: 1077546314564781.

Yang JN, Wu JC, Agrawal AK, et al. (1994) Sliding mode control for seismic-excited linear and nonlinear civil engineering structures. Technical Report NCEER, US National Center for Earthquake Engineering Research, USA.

Yang JN, Wu JC and Agrawal AK (1995a) Sliding mode control for seismically excited linear structures. *Journal of engineering mechanics* 121: 1386–1390.

Yang JN, Wu JC and Agrawal AK (1995b) Sliding mode control for nonlinear and hysteretic structures. *Journal of Engineering Mechanics* 121: 1330–1339.

Yang JN, Wu JC, Reinhorn AM, et al. (1996) Experimental verifications of H∞ and sliding mode control for seismically excited buildings. *Journal of Structural Engineering* 122: 69–75.

Yau JD (2009) Response of a train moving on multi-span railway bridges undergoing ground settlement. *Engineering Structures* 31: 2115–2122.

Yeh YK and Mo YL (2005) Shear retrofit of hollow bridge piers with carbon fiber-reinforced polymer sheets. *Journal of Composites for Construction* 9: 327–336.

Zaghi AE, Saiidi MS and Mirmiran A (2012) Shake table response and analysis of a concrete-filled FRP tube bridge column. *Composite Structures* 94: 1564–1574.

Zhang J, Huo Y, Brandenberg SJ, et al. (2008) Effects of structural characterizations on fragility functions of bridges subject to seismic shaking and lateral spreading. *Earthquake Engineering and Engineering Vibration* 7: 369–382.

Zou L, Huang K, Wang L, et al. (2012) Vibration control of adjacent buildings considering pile-soil-structure interaction. *Journal of Vibration and Control* 18: 684–695.